Origins of plasma filamentation in high intensity laser fields and specific time-scale estimation

ALEXEI ZUBAREV[a,*], MARINA CUZMINSCHI[b,c], ANA-MARIA IORDACHE[d]
[a]*National Institute for Laser, Plasma and Radiation Physics, Magurele, Ilfov, Romania*
[b]*University of Bucharest, Faculty of Physics, Magurele, Ilfov, Romania*
[c]*"Horia Hulubei" National Institute for Physics and Nuclear Engineering, 30 Reactorului, Magurele, Ilfov, Romania*
[d]*National Institute of Research and Development for Optoelectronics – INOE 2000, Magurele, Ilfov, Romania*

Recent experiments confirm the generation of long-living stable current filaments during plasma-laser interaction. In this paper, we theoretically deduce and numerically study the time of plasma-laser interaction required for filaments generation. We assume that plasma filaments appear due to non-uniform growth of Weibel instability at vacuum - overdense plasma interface. We deduce the minimal pulse duration for which filaments appear as function of laser intensity. The results obtained in our study are in agreement with previous experiments and numerical simulations. Finally, we notice that generation of plasma filaments is hard to observe at experiments at CETAL, but will influence experiments performed at ELI.

(Received September 10, 2020; accepted October 7, 2021)

Keywords: Plasma-laser interaction, Filamentation, Weibel instability, High-intensity laser, Time-scale

1. Introduction

Since their discovery, lasers were used for production of localized plasma [1] and charged particles beams [2,3] with direct applications both in science and art [4]. However, until application of chirped pulse amplification method [5,6] laser power was not high enough for the study of strong collective phenomena in plasma. Since 1990 the power of big lasers grows exponentially and now rises up to 1 PW in 2018 for CETAL [7], PHELIX PW laser [8] and VULCAN PW laser [9]. First experiments performed at ELI-NP showed record power of 10 PW [10].

Generated by high intensity laser radiation plasma instabilities are of interest for both applicative and fundamental research [11]. High intensity lasers are used for simulation of astrophysical phenomena [12] and generation of high energy particle beams [13], with numerous applications in inertial confinement [14], proton imaging [15] and nuclear physics [16].

Emission of high energy particles is a perspective technology due to compact dimensions of plasma-laser accelerators [17]. Plasma-laser accelerators provide high quality electron beams [18,19] and in perspective can be used for generation of ultra-short proton beams [20]. Main mechanisms invoiced in electron acceleration process are direct laser acceleration and laser wakefield acceleration [21]. Protons are accelerated by secondary fields generated in plasma due to the plasma polarization and electron waves generation [22].

For low intensity lasers the main mechanism of particle acceleration is direct laser acceleration, and plasma can be considered just a source of the particles [17]. However, with the increase of laser power and improvements of their focusing, internal processes in plasma become important and significantly change the energetic spectra of particles beam [23].

According to recent numerical [24,25] and experimental [26] investigations plasma acquires non-uniform structure, different types of waves are generated and instabilities appear [27,28,29]. This leads to a set of complex non-linear phenomena and plasma behavior becomes chaotic [30].

Long living structures generated in plasma in some experiments [23,31] have a strong influence on the energetic spectra of emitted particles. Such structures can be defined as plasma filaments characterized by high temperature, and current density. Moreover, similar structures were obtained during numerical simulations [25,30,32].

Experiments effectuated at VULCAN laser facility [23] used proton imaging to obtain a real time evolution of plasma irradiated with high-intensity laser pulse. Was observed spatial expansion of plasma and generation of plasma filaments. The current filaments appears due to energy transfer from electrons to photons. Plasma spatial expansion changes from an ordered to a chaotic one and produces electron and ion instabilities with different growth rate.

Such behavior is hard to describe analytically and usually numerical simulations [23,25,33] or some phenomenological models [33] are used.

The main influence of coherent radiation consists in Lorentz force applied to the electrons in plasma. The process leads to massive ionization with further generation of secondary fields. These phenomena take place at lowest spatial scale. Low scale phenomena in laser driven plasma plays an important role in synthesis of periodic nanostructures [34] and graphene quantum dots [35,36]. Subsequently at the upper scales, a special role is played by

small fluctuations in field and charge carries velocity distribution for the generation of plasma instabilities.

As in the other open systems [37,38], we can observe the phase transition in the plasma produced by high-intensity laser radiation when the energy flux through the system increases. It leads to change in transport properties, spatial energy distribution and entropy production [39]. From the electrodynamic point of view this process is associated with magnetic reconnection [40].

Magnetic reconnection takes place in plasma, when two magnetic lines are cut and reconnected in a different way. The topological structure of the field changes during the magnetic reconnection. According to the Taylor principle [40,41] the potential energy of the field is minimized, and the kinetic energy of plasma increases. After the reconnection, the rate of entropy production decreases and large scale instabilities appears.

Further development of large scale instabilities occurs in accordance with the principle of minimum entropy production due to energy transfer from low to large scales [33]. This process is similar to the energy cascade but occurs in a single step by direct coupling between low and large scale instabilities. In Ref. [33] it is described as energy transfer from quasi-particles associated with short wavelength packages waves produced by collective large scale instabilities.

In this article we study the origins of plasma filaments generated in high-intensity laser field, estimate the time of their generation as a function of laser radiation intensity, and verify the generation of filaments for the most powerful worldwide lasers. The work we performed shows the importance of the pulse duration for the plasma laser interaction experiments, and the possibility to use the long laser pulse duration to obtain high energy plasma channels.

2. Model and method

Phenomena that happen during plasma-laser interaction during plasma laser interaction has place at different scales.

As a result of changes in characteristics of a plasma (like temperature, magnetic fields, electric fields, density) a turbulence region may appear. It is called plasma instability, which can belong to hydrodynamic or kinematic group. Weibel instability occurs due to strong magnetic fields in a plasma movement appear collisionless shocks and have been observed in laser experiments [42]. At low scale in case of plasma-laser interaction, the Weibel instability is the predominant instability that appears. Connection between plasma filamentation and Weibel instability was established in the article [23].

Transverse electromagnetic waves, which contain electrons of plasma alone and spontaneously produced in plasma as a result of an amply anisotropic velocity distribution were first theoretically deduced by Erich S. Weibel [43] in 1958. It was derived using the Boltzmann transport equation omitting the collision term and keeping only linear terms of the perturbation:

$$\frac{\partial f}{\partial t}+\vec{\mathrm{v}}\cdot\frac{\partial f}{\partial \vec{r}}+\frac{e}{m}\left[\vec{\mathrm{v}}\times\vec{B}_0\right]\cdot\frac{\partial f}{\partial \vec{\mathrm{v}}} =-\frac{e}{m}\left[\vec{E}+\vec{\mathrm{v}}\times\vec{B}\right]\cdot\frac{\partial f_0}{\partial \vec{\mathrm{v}}} \tag{1}$$

where f is the perturbation of the distribution function, $\vec{B}_0$ represents constant magnetic field, $f_0(\vec{\mathrm{v}})$ is a nonisotropic distribution that is in our case stationary and $\vec{E}$ and $\vec{B}$ depict perturbation of the electromagnetic field. Let us consider the case when $f(\vec{\mathrm{v}},\vec{r},t),\vec{E}(\vec{r},t),\vec{B}(\vec{r},t)$ are of form $\exp(i\omega t+i\vec{k}\cdot\vec{r})$ in $\vec{r}$ and t. In this case eliminating $\vec{B}$ using homogeneous Maxwell equations we get:

$$i(\omega+\vec{\mathrm{k}}\cdot\vec{\mathrm{v}})f-\frac{e\vec{B}_0}{m}\cdot\left[\vec{\mathrm{v}}\times\frac{\partial f}{\partial \vec{\mathrm{v}}}\right] =-\frac{e}{m\omega}\left\{\omega\vec{E}\cdot\frac{\partial f_0}{\partial \vec{\mathrm{v}}}+\left[\vec{k}\times\vec{E}\right]\cdot\left[\vec{\mathrm{v}}\times\frac{\partial f_0}{\partial \vec{\mathrm{v}}}\right]\right\} \tag{2}$$

The effects of anisotropy are included in the term $-e/(m\omega)[\vec{\mathrm{k}}\times\vec{\mathrm{E}}]\cdot[\vec{\mathrm{v}}\times\partial f_0/\partial\vec{\mathrm{v}}]$. The constant magnetic field is not the primary source in the appearance of instabilities. The solution of equation (2) for $\vec{B}_0$ and $\vec{\mathrm{k}}$ aligned along Z-axis, $\vec{E}$ is perpendicular to them, and:

$$f_0(\vec{\mathrm{v}})=\mathrm{F}(v_o,v_z),v_0^2=v_x^2+v_y^2,$$

is:

$$f=\frac{e\left\{i(\omega+kv_z)(v_x\,\mathrm{E}_x+v_y\,\mathrm{E}_y)+(\frac{\mathrm{eB}_0}{m})(v_x\,\mathrm{E}_y-v_y\,\mathrm{E}_y)\right\}}{m\omega v_0\left\{(\frac{eB_0}{m})^2-(\omega+\mathrm{k}\,v_z)^2\right\}} \times\left\{kv_0\frac{\partial f_0}{\partial v_z}-(\omega+\mathrm{k}\,v_z)\frac{\partial f_0}{\partial v_0}\right\}$$

Taking into consideration the equations:

$$\delta=e\int f(\vec{\mathrm{v}},\vec{r},t)d^3v;\qquad \vec{j}=e\int\vec{\mathrm{v}}\,f(\vec{\mathrm{v}},\vec{r},t)d^3v \tag{3}$$

Maxwell equations and eradicating the fields $\vec{E}$ and $\vec{B}$ we have:

$$k^2-\omega^2=\frac{e^2}{m}\pi\int_{v_0=0}^{\infty}\int_{v_3=-\infty}^{\infty}\frac{(\omega+\mathrm{k}v_3)\frac{\partial f_0}{\partial v_0}-v_0k\frac{\partial f_0}{\partial v_3}}{(\omega+kv_3\pm(\frac{eB_0}{m}))}\times v_0^2dv_0dv_3 \quad (4)$$

Let us consider the distribution function given by:

$$f_0=\frac{n}{u_0^2u_3(2\pi)^{3/2}}\exp[-\frac{v_0^2}{2u_0^2}-\frac{v_3^2}{2u_3^2}] \quad (5)$$

then we get:

$$\mathrm{k}^2-\omega^2=\omega_p^2\left\{A-(\mathrm{A}\frac{\omega\pm\omega_c}{u_3k}+\frac{\omega}{u_3k})\phi(\frac{\omega\pm\omega_c}{u_3k})\right\} \quad (6)$$

with

$$\phi(\mathrm{z})=\exp(-\frac{1}{2}\mathrm{z}^2)\int_{-i\infty}^{z}\exp(\frac{1}{2}\xi^2)d\xi \quad (7)$$

and

$$\omega_p^2=\frac{ne^2}{m},\omega_c=\frac{eB_0}{m},A=(\frac{u_0}{u_3})-1 \quad (8)$$

According to Ref. [44] the growth rate of Weibel instability is:

$$\gamma W(k)=k(\frac{T_{\square 0}}{m_e}\frac{P-\frac{c^2k^2}{\omega_{pe}^2}}{1+(-\frac{c^2k^2}{\omega_{pe}^2})})^{1/2} \quad (9)$$

After secondary magnetic field generated by Weibel instability becomes strong enough and reaches the critical value, magnetic reconnection occurs. It is described by the following mechanism [40,41]

In the case of quasi-collisionless conditions, the fluid characterization of plasma is a good approximation of the bulk behavior. We will take into consideration the long-wavelength regime $\lambda \gg \lambda_D$ (λ_D is the Debye length). In this instance we are dealing with quasi-neutral limit. The continuity equation in case of one slightly charged ion group is:

$$\partial_t n=-\nabla\cdot\vec{\mathrm{v}}_i\,n=-\nabla\cdot\vec{\mathrm{v}}_e\,n \quad (10)$$

Under these conditions, the equations of motions are:

$$m_in(\partial_t\vec{\mathrm{v}}_i+\vec{\mathrm{v}}_i\cdot\nabla\vec{\mathrm{v}}_i)=$$
$$-\nabla\mathrm{p}_i+en(\vec{\mathrm{E}}+\frac{\mathrm{v}_i}{c}\times\vec{\mathrm{B}})-\nabla\cdot\pi_i-ne\eta\vec{j} \quad (11)$$

and

$$m_en(\partial_t\vec{\mathrm{v}}_e+\vec{\mathrm{v}}_e\cdot\nabla\vec{\mathrm{v}}_e)=$$
$$-\nabla\mathrm{p}_e+en(\vec{\mathrm{E}}+\frac{\mathrm{v}_e}{c}\times\vec{\mathrm{B}})-\nabla\cdot\pi_e-ne\eta\vec{j} \quad (12)$$

with $p_{i,e}$ being the scalar pressures, $\pi_{e,i}$ is the stress tensor, η is the scalar resistivity and $\vec{j}=ne(\vec{\mathrm{v}}_i-\vec{\mathrm{v}}_e)$ is the current density. We assume that $\pi_{e,i}$ are small and:

$$\nabla\cdot\pi_{i,e}=n\mu_{i,e}\nabla^2\vec{\mathrm{v}}_{i,e}$$

with $\mu_{i,e}$ being scalar viscosities. The pressures follow the adiabatic law:

$$\partial_t p_{i,e}+\vec{\mathrm{v}}_{i,e}\cdot\nabla p_{i,e}=-\gamma p_{i,e}\nabla\cdot\vec{\mathrm{v}}_{i,e} \quad (13)$$

We obtain the mass flow expression by summing (11) and (12) $\vec{v}=\frac{m_i\vec{v}_i+m_e\vec{v}_e}{m_i+m_e}\cong\vec{v}_i$ and omitting the electric field gives us:

$$m_in(\partial_t\vec{\mathrm{v}}+\vec{\mathrm{v}}\cdot\nabla\vec{\mathrm{v}})=-\nabla p+\frac{1}{c}\vec{j}\times\vec{B}-\nabla\cdot\pi_i \quad (14)$$

where we used $p=p_i+p_e$ and $\pi_i+\pi_e\cong\pi$.We write the generalized Ohm's law:

$$\vec{E}+\frac{\vec{\mathrm{v}}}{c}\times\vec{B}=\vec{R} \quad (15)$$

with $\vec{R}$ including the rest of the terms. Now let us use normalizations $x/\mathrm{L},v/v_A,t/t_A$ where L is a spatial scale, $v_A=\frac{B_0}{\sqrt{4\pi nm_i}}$, $t_A=L/v_A$. This way, the expression of equation (14) becomes:

$$\vec{R}=\eta\vec{j}+\mu_e\nabla^2\vec{\mathrm{v}}_e+d_i[\vec{j}\times\vec{B}-\beta\nabla p_e-\mathrm{d}_e^2(\partial_t\vec{\mathrm{v}}_e+\vec{\mathrm{v}}_e\cdot\nabla\vec{\mathrm{v}}_e)] \quad (16)$$

where ion and electron inertia scales are d_i and d_e, β is the measure of the plasma pressure distinguished from the magnetic pressure, η is the normalized resistivity and μ_e is dimensionless electron viscosity. In the large scale $\vec{R}$ is small and in this way we obtain:

$$\partial_t\vec{B}=\nabla\times(\vec{\mathrm{v}}\times\vec{B}) \quad (17)$$

Therefore, we have obtained the main expressions in context of magnetohydrodynamics (MHD). It is specific for highly conducting plasma to conserve the magnetic flux

across a surface *F(t)* bounded by a curve *l(t)* shifting with the fluid:

$$\frac{d}{dt}\int \vec{B}d\vec{F} = \int_F \partial_t \vec{B}\cdot d\vec{F} + \int_{\partial_t F} \vec{B}\cdot d\vec{F}$$
$$= \int_F \nabla\times(\vec{\mathrm{v}}\times\vec{B})\cdot d\vec{F} + \int_l \vec{B}\cdot(\vec{\mathrm{v}}\times d\vec{l}) = 0 \quad (18)$$

On the other hand, observations without any doubt illustrate that most dynamic processes in plasmas include an alteration in field line topology, for example field lines have to reconnect after being cut. In our case, we are interested in reconnection via a dissipative process, therefore the terms in eq. (15) proportional to d_i are ignored and $\vec{R} \cong \eta\vec{J}$. Reconnecting motions are incompressible, meaning that $\nabla\cdot\vec{\mathrm{v}} = 0$ and $n = n_0$. Taking curl of eq. (13a) and using the same normalizations, incompressible resistive MHD equations become:

$$\partial_t\vec{\omega} - \nabla\times(\vec{\mathrm{v}}\times\vec{B}) - \nabla\times(\vec{\mathrm{j}}\times\vec{B}) = \mu_i\nabla^2\vec{\omega} \quad (19)$$

$$\partial_t\vec{B} - \nabla\times(\vec{\mathrm{v}}\times\vec{B}) = \eta\nabla^2\vec{B} \quad (20)$$

$$\nabla\cdot\vec{\mathrm{v}} = \nabla\cdot\vec{B} = 0, \vec{\omega} = \nabla\times\vec{\mathrm{v}}, \vec{j} = \nabla\times\vec{B}$$

where $\vec{\omega}$ is the vorticity.

Let us consider quasi-stationary resistive reconnection. When the Reynolds number $R_m \gg 1$ fast reconnection takes place when the gradients scales of reconnection are shorter than the global scale. The process of reconnection is localized around small convective term areas. Fig. 1 depicts what happens in the vicinity of these points. We are taking a look at the case when plasma moves from above and below and evacuates to the side. This structure has a high chance to be flattened into a sheet.

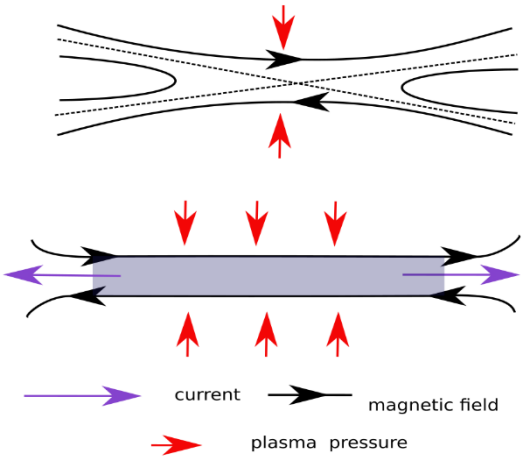

Fig. 1. Schematic representation of magnetic reconnection (color online)

Magnetic reconnection can be considered a second order phase transition in plasma. The thermodynamical properties of plasma changes [39].

During the evolution of plasma entropy in magnetic tubes is conserved $S = PB^{\gamma}$. And effective temperature of the plasma can be calculated using the formula:

$$\tilde{T}k_B = \int E\tilde{f}_0(E, a=0)dE = \int Ef_1(E, a=a_1)dE \quad (21)$$

where *a* is the parameter that indicate how far is the distribution from the equilibrium.

After the magnetic reconnection takes place, we can describe the growing of filaments by energy pumping mechanism [33]. We consider that the filament as large scale instability, which is pumped by low scale instabilities described in this formalism as quasi-particles.

The dispersion relation of electrostatic waves in turbulent plasma in terms of quasiparticle susceptibility is:

$$\varepsilon(\omega, \vec{\mathrm{k}}) = -\chi_{qp} \quad (22)$$

In case of perturbation on potential ϕ and perturbed distribution $\tilde{N}(\vec{k}')$ of the form $\mathrm{e}^{\mathrm{i}(\vec{k}\cdot\vec{r}-\omega t)}$ we have:

$$\varepsilon(\omega, \vec{\mathrm{k}})\phi = \int g(\vec{\mathrm{k}}, \vec{\mathrm{k}}')\tilde{N}(\vec{\mathrm{k}}')d\vec{\mathrm{k}}' \quad (23)$$

In our case, quasiparticle number density does not depend on frequency and corresponding Liouville's theorem is:

$$\frac{d}{dt}N(\vec{\mathrm{k}}') = \left(\frac{\partial}{\partial t} + \vec{v}'\cdot\frac{\partial}{\partial\vec{r}} + \vec{\mathrm{F}}'\cdot\frac{\partial}{\partial\vec{k}'}\right)\mathrm{N}(\vec{\mathrm{k}}') = 0 \quad (24)$$

where the quasiparticle velocity is $\vec{v}' = \frac{\partial\omega}{\partial\vec{k}'}$ and $\vec{F}' = \frac{d\vec{k}'}{dt}$ is the force caused by perturbations acting on quasiparticles.

Using the notation $f(\vec{k}, \vec{k}') = f'(\vec{k})g(\vec{k}, \vec{k}')$ and $N(\vec{k}') = N_0(\vec{k}') + \tilde{\mathrm{N}}(\vec{k}')$ we obtain:

$$\varepsilon(\omega, \vec{k}) = -\int f(\vec{k}, \vec{k}')\frac{\vec{k}\cdot\frac{\partial N_0}{\partial\vec{k}'}}{\omega - \vec{k}\cdot\vec{v}'}d\vec{k}' \quad (25)$$

3. Phenomenological model

Following the interaction between the high-intensity laser radiation and the solid target different processes occur. Field intensity reaches $I > 10^{19}$W/cm^2 yielding in nearly instantaneous ionization. Therefore, we can focus on the interaction between the laser pulse and the over-dense

plasma. The gradual generation of long-range instabilities is shown in the Fig. 2.

The highest frequency in plasma corresponds to the oscillations of laser fields and is assumed to be ω_0. All other processes have much lower frequencies. Generation of low scale instabilities has place due to fluctuations in magnetic field. At this scale plasma behavior is determinated by Weibel instability with growth rate:

$$\gamma(k) = k\left(\frac{T_0}{m_e}\frac{P - \frac{c^2k^2}{\omega_{pe}^2}}{1+\frac{c^2k^2}{\omega_{pe}^2}}\right)^{1/2} \tag{26}$$

This dependence is almost linearly for large range of k, so we can assume that the characteristic time for low scale instabilities is $t_1 = \varepsilon\omega_0^{-1}$, where $\varepsilon \sim \frac{1}{B}$.

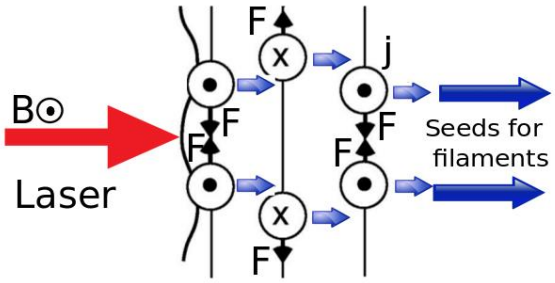

Fig. 2. Formation of seeds for plasma filaments from Weibel instability (color online)

In Fig. 2 is shown the growth of Weibel instability, with generation of low scale currents. Due to magnetic field associated with laser radiation ponderomotive force appears. And plasma becomes inhomogeneous. Each local current channel is a potenial seed for large scale filament.

At the upper time scale with specific period $t_2 = \varepsilon^2\omega^{-1}$ we should take into account non-uniform growth rate of Weibel instabilities in different places of plasma vacuum interface. It happens due to fluctuations in laser field and Gaussian distribution of intensity in laser spot.

When the secondary magnetic in most developed current channels reaches a critical value, magnetic reconnection occurs. The exact value is hard to estimate analytically, however by analyzing numerical or experimental data we can observe a second order phase transition, and sudden change in entropy production rate.

Reconnection helps growth of large scale instabilities.

And further growth occurs without supplementary energy flux from laser pulse. So the minimal pulse duration necessarily for generation of long living filaments is given by the magnetic reconnection moment. It is given by the relation:

$$\tau_{\min} = \varepsilon^2\omega_0^{-1} = \alpha I^{-1/4} \tag{27}$$

where I is laser field intensity and αI is an empiric constant.

4. Experimental data analysis and discussion

To confirm the theoretical model and to find empirical constants we used the results of experiments and massive numerical simulations implemented at Vulcan laser presented in Ref. [32].

First, we extracted the profiles of magnetic field generated in plasma at different moments of time (Fig. 3). We observe that the amplitude of field oscillations remains constant up to a time threshold, after which the value increase fast.

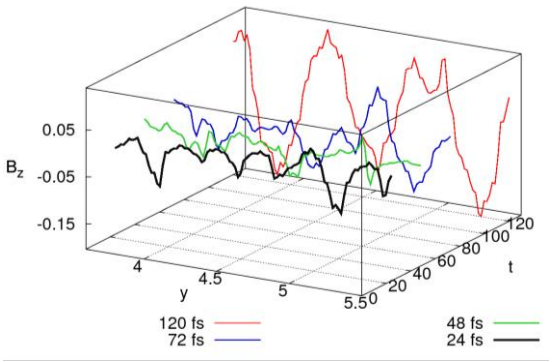

Fig. 3. Profiles of magnetic fields for different times extracted from numerical data presented in Ref. [32] (color online)

The obtained results were used to estimate potential energy in plasma and the entropy density. From Fig. 4 we observe that $S(x)$ has almost constant value at the begin of laser pulse and a minimum appears. Local decrease of entropy in an open system show that self-organization takes place. Local decrease of entropy occurs in according with the formula:

$$\tilde{S}_0 - S_1 = \int \log\left(\frac{f_1(\mathrm{E})}{\tilde{f}_0(\mathrm{E})}\right) f_1(\mathrm{E})\,\mathrm{dE} \geq 0 \tag{28}$$

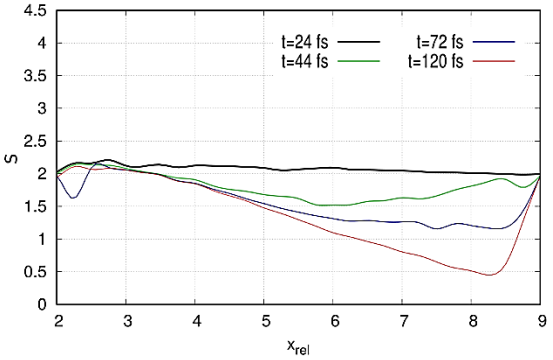

Fig. 4. Evolution of entropy density profile S(x) during plasma filamentation in experiment described in Ref. [32] (color online)

The evolution of average magnetic field induction in time is presented in Fig. 5 (a). We observed that the average magnetic field induction and respectively the potential energy of plasma increase monotonically. We have not noticed any time threshold in the average magnetic field evolution.

Moreover we calculated the energy per entropy density ratio (Fig. 5(b)), E/S, that increases monotonically too. However, we can observe that the rate of entropy production significantly decreases at 65 fs. This time can be associate with the generation of the plasma filaments from the low scale Weibel instability fields. The evolution of the electromagnetic field energy and the energy per entropy ratio allow us to specify the process as a second order phase transition.

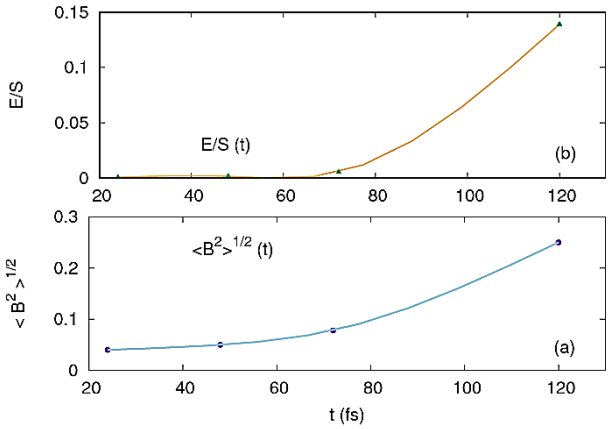

Fig. 5. Dependence of average magnetic field (a) and energy per entropy density ratio on time for numerical data presented in Ref. [32] (color online)

Using the results from Fig. 5 (b) we estimated the delay of between start of laser pulse and generation of plasma filaments (Fig. 6). For lasers with pulse duration greater then indicated by continuous line filamentation occurs. For CETAL laser filamentation can occur in favorable conditions but the result of experiment is determined by fluctuations. For ELI filamentation will play an important role.

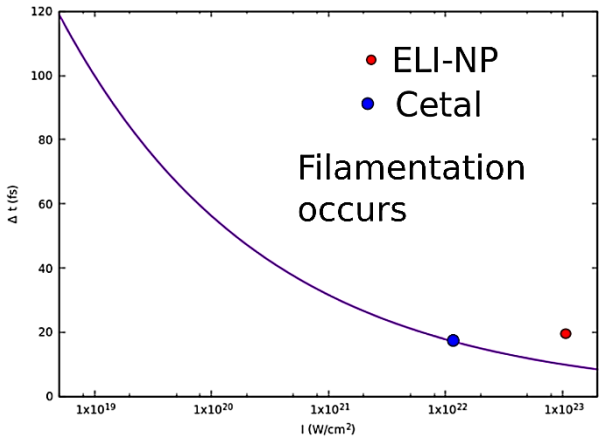

Fig. 6. Filamentation at biggest Romanian lasers (color online)

In the experiments effectuated on the ELI-NP laser installation filamentation will play an important role and can significantly perturb the experimental results.

5. Conclusions

Usually, it is considered that a combination of high laser power and short pulse duration is the unique way to obtain extremely high energy density in plasma and respectively to produce high energy particle beams. However, plasma filamentation occurs when a solid target is irradiated by a high-intensity laser pulse and generates high energy density regions in plasma due to self-organization. It favors emission of high energy beams and improve perforation of hypothetic plasma accelerator. To obtain long living plasma filaments the following relation between pulse duration τ and laser intensity I should be satisfied $\tau > \alpha^2 I^{-1/4} \omega^{-1}$, where α is an empiric constant and ω is the frequency of laser radiation. Phenomenological model proposed in this article describes generation of plasma filaments in three steps: first low scale instabilities as Weibel instability grows, after due to nonuniform growing seeds for further filaments become more pronounced and at the last step magnetic reconnection occurs. After the reconnection the filaments grow due to energy pumping mechanism according to principle of minimal entropy production. The results were confirmed using experimental and numerical data. The obtained pulse duration, and laser power relationship, allow easily to predict qualitatively the results of experiments on the powerful laser installations and help to choose optimal parameters for plasma laser interaction experiments.

Acknowledgements

A.Z. acknowledges the financial support from the Project 16N/08.02.2019. A.M.I. was funded by a grant of the Romanian Ministry of Education and Research, CNCS - UEFISCDI, project number PN-III-P1-1.1-PD-2019-1134 (ctr. 87/2020), within PNCDI III.

References

[1] W. I. Linlor, Bull. Am. Phys. Soc. **7**, 440 (1958).
[2] R. E. Honig, J. R. Woolston, App. Phys. Lett. **2**(7), 138 (1963).
[3] W. I. Linlor, I. William, App. Phys. Lett. **3**(11), 210 (1963).
[4] L. Angheluta, A. Moldovan, R. Radvan, U. P. B. Sci. Bull., series A **73**(4), 193 (2011).
[5] M. Pessot, P. Maine, G. Mourou, Opt. Commun. **42**(6), 419 (1987).
[6] P. Maine, D. Strickland, P. Bado, M. Pessot, G. Mourou, IEEE J. Quantum. Electron. **24**(2), 398 (1998).
[7] O. Budriga, E. D'Humieres, Laser. Part. Beams **35**(3), 458 (2017).

[8] P. Hilz, T. M. Ostermayr, A. Huebl, V. Bagnoud, D. Borm, M. Bussmann, M. Gallei, J. Gebhard, D. Haffa, J. Hartmann, T. Kluge, Nat. Com. **9**(1), 1 (2018).
[9] A. G. Krygier, J. T. Morrison, R. R. Freeman, H. Ahmed, J. A. Green, A. Alejo, S. Kar, L. Vassura, APS Meet. Abs. **BO** 5-015 (2014).
[10] V. Zamfir, K. Tanaka, C. Ur. Europhys. News. **50**(2), 23 (2019).
[11] T. P. Hughes, Plasmas and laser light, NYMP, 100 (1975).
[12] B. A. Remington, A. David, R. Paul, H. Takabe, Science **284**(5419), 1488 (1999).
[13] W. Leemans, E. Esarey, Phy. Today **62**(3), 44 (2009).
[14] R. Betti, O. A. Hurricane, Nat. Phys. **12**(5), 435 (2016).
[15] T. E. Cowan, J. Fuchs, H. Ruhl, A. Kemp, P. Audebert, M. Roth, R. Stephens, I. Barton, A. Blazevic, E. Brambrink, J. Cobble, Phys. Rew. Lett. **92**(20), 204801 (2004).
[16] F. Gobet, C. Plaisir, F. Hannachi, M. Tarisien, T. Bonnet, M. Versteegen, M. M. Aléonard, G. Gosselin, V. Méot, P. and Morel, Nucl. Instrum, Meth. A **653**(1), 80 (2011).
[17] V. Malka, J. Faure, A. G. Yann, E. Lefebvre, A. Rousse, K. T. Phuoc, Nat. Phys. **4**(6), 447 (2008).
[18] S. Mangles, C. D. Murphy, Z. Najmudin, A. G. R. Thomas, J. P. Collier, A. E. Dangor, E. J. Divall, P. S. Foster, J. G. Gallacher, C. J. Hooker, D. A. Jaroszynski, A. J. Langley, W. B. Mori, P. A. Norreys, F. S. Tsung, R. Viskup, B. R. Walton, K. Krushelnick, Nat. **431**(7008), 535 (2004).
[19] N. A. Hafz, T. M. Jeong, I. W. Choi, S. K. Lee, K. H. Pae, V. V. Kulagin, J. H. Sung, T. J. Yu, K. H. Hong, T. Hosokai, T. J. R. Cary, Nat. Phot. **2**(9), 571 (2008).
[20] S. Fourmaux, S. Buffechoux, B. Albertazzi, D. Capelli, A. Lévy, S. Gnedyuk, L. Lecherbourg, P. Lassonde, S. Payeur, P. Antici, H. Pépin, R. S. Majoribanks, J. Fuchs, J. C. Kieffer, Phys. Plasmas **20**(1), 013110 (2013).
[21] A. Caldwell, K. Lotov, A. Pukhov, F. Simon, Nat. Phys. **5**(5), 363 (2009).
[22] R. L. Williams, C. E. Clayton, C. Joshi, T. Katsouleas, W. B. Mori, Laser Part. Beams **8**(3), 427 (1990).
[23] K. Quinn, L. Romagnani, B. Ramakrishna, G. Sarri, M. E. Dieckmann, P. A. Wilson, J., Fuchs, L. Lancia, A. Pipahl, T. Toncian, O. Willi, Phys. Rev. Lett. **108**(13), 135001 (2012).
[24] A. O'Neill, Laser Wakefield Accelerator Simulations Using EPOCH, Queen's University Belfast (2017).
[25] O. Culfa, G. J. Tallents, A. K. Rossall, E. Wagenaars, C. P. Ridgers, et al. Phys. Rev. E, **93**(4), 043201 (2016).
[26] T. E. Geints, A. A. Ionin, D. V. Mokrousova, G. E. Rizaev, L. V. Seleznev, E. S. Sunchugasheva, A. A. Zemlyanov, Journal of the Optical Society of America **36**(10), G19 (2019).
[27] D. S. Montgomery, Phys. Plasmas **23**(5), 055601 (2016).
[28] C. Negutu, M. Stafe, S. S. Ciobanu, N. N. Puscas, J. Optoelectron. Adv. M. **13**(7-8), 812 (2011).
[29] N. Banu, D. Toader, M. L. Munteanu, A. Scurtu, C. M. Ticos, J. Optoelectron. Adv. M. **15**(9-10), 976 (2013)
[30] S. Sharma, N. Kumar, S. Hussain, R. P. Sharma, Laser Part. Beams **35**(1), 10 (2017).
[31] F. Pegoraro, Phys. Scr. **63**, 262 (1996).
[32] Y. Sentoku, K. Mima, S. Kojima, H. Ruhl, Phys. Plasmas **7**(2), 689 (2000).
[33] J. T. Mendonça, R. Bingham, P. K. Shukla, Phys. Rev. E **68**(1), 016406 (2003).
[34] T. Shinonaga, S. Kinoshita, Y. Okamoto, A. Okada., ICALEO, Laser Institute of America, **2016**(1), (2016).
[35] A. Tiliakos, A. M. Trefilov, E. Tanasă, A. Balan, I. Stamatin, Appl. Surf. Sci. **504**, 144096 (2020).
[36] A. Tiliakos, C. Ceaus, S. M. Iordache, E. Vasile, I. Stamatin, J. Anal. Appl. Pyrol. **121**, 275 (2016).
[37] M. Cuzminschi, A. Zubarev, Crystals **9**(7), 327 (2019).
[38] M. Cuzminschi, R. Gherasim, V. Girleanu, A. Zubarev, I. Stamatin, Energ Buildings **158**, 964 (2018).
[39] R. L. Dewar, M. J. Hole, M. McGann, R. Mills, R. S. R. Hudson, 2008. Entropy **10**(4), 621 (2008).
[40] J. Taylor, Rev. Mod. Phys. **58**(3), 741 (1986).
[41] D. Biskamp, Astrophys. Space Sci. **242**(1-2), 165 (1996).
[42] C. M. Huntington, F. Fiuza, J. S. Ross, A. B. Zylstra, R. P. Drake, D. H. Froula, G. Gregori, N. L. Kugland, C. C. Kuranz, M. C. Levy, C. K. Li, J. Meinecke, T. Morita, R. Petrasso, C. Plechaty, B. A. Remington, D. D. Ryutov, Y. Sakawa, A. Spitkovsky, H. Takabe, H.-S. Park Nature Physics **11**(2), 173 (2015).
[43] E. S. Weibel, Phys. Rev. Lett. **2**(3), 83 (1959).
[44] V. Yu. Bychenkov, V. P. Silin, V. T. Tikhonchuk, Phys. Lett. A **138**, 127 (1989).

*Corresponding author: alxzubarev@gmail.com